Journal of Solid State Chemistry 195 (2012) 94–100

Contents lists available at SciVerse ScienceDirect

Journal of Solid State Chemistry

journal homepage: www.elsevier.com/locate/jssc

Novel 3D bismuth-based coordination polymers: Synthesis, structure, and second harmonic generation properties

Arief C. Wibowo [a], Mark D. Smith [a], Jeongho Yeon [b], P. Shiv Halasyamani [b], Hans-Conrad zur Loye [a,*]

[a] Department of Chemistry and Biochemistry, University of South Carolina, 631 Sumter Street, Columbia, SC 29208, USA
[b] Department of Chemistry, University of Houston, 136 Fleming Building, Houston, TX 77204-5003, USA

ARTICLE INFO

Available online 16 February 2012

Keywords:
Coordination polymer
Polar structure
Second harmonic generation

ABSTRACT

Two new 3D bismuth containing coordination polymers are reported along with their single crystal structures and SHG properties. Compound **1**: $Bi_2O_2(pydc)$ (pydc=pyridine-2, 5-dicarboxylate), crystallizes in the monoclinic, polar space group, $P2_1$ (a=9.6479(9) Å, b=4.2349(4) Å, c=11.9615(11) Å, β=109.587(1)°), which contains Bi_2O_2 chains that are connected into a 3D structure via the pydc ligands. Compound **2**: $Bi_4Na_4(1R3S\text{-cam})_8(EtOH)_{3.1}(H_2O)_{3.4}$ (1*R*3*S* cam=1*R*3*S*-camphoric acid) crystallizes in the monoclinic, polar space group, $P2_1$ (a=19.0855(7) Å, b=13.7706(5) Å, c=19.2429(7) Å, β=90.701(1)°) and is a true 3D coordination polymer. These are two example of SHG compounds prepared using unsymmetric ligands (compound **1**) or chiral ligands (compound **2**), together with metals that often exhibit stereochemically-active lone pairs, such as Bi^{3+}, a synthetic approach that resulted in polar, non-centrosymmetric, 3D metal-organic coordination polymer.

1. Introduction

Metal-Organic Materials (MOMs) contain metal moieties and organic ligands that together form discrete or polymeric structures that can be one-, two-, or three-dimensional, and that display various properties resulting from the presence of the metal moieties and/or ligand connectors [1]. Three-dimensional extended structures with permanent porosity, considered as second generation MOMs, are commonly known as metal-organic frameworks, a term coined by Yaghi [2, 3], or, alternatively, porous coordination polymers, as proposed by Kitagawa [4, 5]. The facile prediction of network topologies was made possible by Yaghi and O'Keeffe who developed the so-called Reticular Chemistry approach in which they exploit the use of secondary building units (SBU) as molecular polyhedra for the construction of well-designed MOFs [6, 7]. With such a rational approach, the "design" of MOMs becomes possible and an unlimited number of MOMs with different structures (network topologies), sizes (pore size, surface area, and resulting particle size), as well as properties (multi-functional MOMs), can be envisioned.

The concept of using nodes and spacers, introduced first by Wells [8–11], to form regular and somewhat predictable network topologies, such as cubic diamondoid, hexagonal diamondoid, square grid, and octahedral network topologies, are commonly observed for transition metals (TMs) and late TMs that form regular metal-organic polyhedra (MOP). This is not the case, however, for main group metals possessing lone pairs, such as Sn^{2+}, Bi^{3+}, and Pb^{2+}, which typically form hemi-directed metal-organic polyhedra (distorted polyhedra) as building blocks. The resulting network topologies, consequently, are not as regular and as predictable as those for the commonly used TM and late TMs (such as Cu^{2+} and Zn^{2+}) systems, which makes the former less explored. In rare cases, however, these lone pair metals can form surprisingly regular network topologies, such as a Kagomé Lattice [12], due to formation of only slightly distorted MOPs (i.e., the lone pairs are not stereochemically-active).

To date, MOMs with a range of functional attributes have been prepared, including record-breaking porosity [13], catalytic properties [14–20], molecular magnetism [21], chemical separations and sensing ability [22, 23], luminescence [24, 25] and NLO properties [26], multiferroic, [27, 28], ferroelectric [29, 30], and switchable molecular dielectric properties [31–33]. For the bismuth-containing Metal–Organic Materials discussed in this paper, the property of interest is second harmonic generation (SHG). A common theme in MOMs with SHG and ferroelectric properties is the formation of non-centrosymmetric (NCS) crystal structures. Some MOMs have been reported having both properties [34–36], while others exhibit only SHG [37–38] or ferroelectric behavior [39]. Note that ferroelectric MOMs have more stringent requirements than those that exhibit only SHG. The former generally posses anomalously high dielectric constants

* Corresponding author. Fax: +1 803 777 8508.
E-mail addresses: zurloye@mail.chem.sc.edu, JSSC@mailbox.sc.edu (H.-C. zur Loye).

0022-4596/$ - see front matter © 2012 Elsevier Inc. All rights reserved.
doi:10.1016/j.jssc.2012.01.038

at the paraelectric to ferroelectric phase transition temperature (Curie temperature, T_C) due to a sudden increase in the spontaneous polarization upon transitioning from the paraelectric, high symmetry phase (generally at high temperature) to the ferroelectric, lower symmetry phase (generally at lower temperature) under an applied electric field.

As continuation of our research in exploring the less investigated main group-based MOMs, herein we report the hydrothermal synthesis of two new 3D bismuth containing coordination polymers, compound **1**: Bi_2O_2(pydc) and compound **2**: Bi_4Na_4(1*R*3*S*-cam)$_8$(EtOH)$_{3.1}$(H_2O)$_{3.4}$, along with their structural characterization and SHG properties.

2. Experimental section

All chemicals were of reagent grade and used without further purification. $Bi(NO_3)_3 \cdot 5H_2O$, pyridine-2, 5-dicarboxylic acid, and 1*R*3*S*-camphoric acid were purchased from Sigma-Aldrich.

2.1. Synthesis of Bi_2O_2(pydc)

A mixture of $Bi(NO_3)_3 \cdot 5H_2O$ (0.242 g, 0.5 mmol) or Bi_2O_3 (0.232 g, 0.5 mmol) and pyridine-2, 5-dicarboxylic acid (H_2pydc) (0.250 g, 1.5 mmol) in H_2O (25 ml) was sealed in a Teflon-lined autoclave and heated to a temperature of 180 °C for 3 day, and then cooled slowly at 0.1 °C/min to room temperature. Colorless, needle-like crystals were obtained in 90% yield (based on bismuth) admixed with an unidentified white powder phase, which was almost completely separated from the needle shaped crystals by sieving. The products were washed with DMF to dissolve and remove any unreacted ligand. The final product was isolated by vacuum filtration. The isolated needle crystals were used for structure and physical characterizations.

2.2. Synthesis of Bi_4Na_4(1R3S-cam)$_8$(EtOH)$_{3.1}$(H_2O)$_{3.4}$

A mixture of $Bi(NO_3)_3 \cdot 5H_2O$ (0.242 g, 0.5 mmol) and an excess of 1*R*3*S*-camphoric acid (1*R*3*S*-cam) (0.300 g, 1.5 mmol) and NaOH (0.024 g, 0.6 mmol) in EtOH (25 ml) was sealed in a Teflon-lined autoclave and heated to a temperature of 100 °C for 3 day, and then cooled slowly at 0.1 °C/min to room temperature. Colorless, needle-shaped crystals and white polycrystalline powder were obtained in quantitative yield based on bismuth. The products were washed with DMF to dissolve and remove any unreacted ligand. The final product was isolated by vacuum filtration. It is this mixture of powder and needle crystals that were used for structure and physical characterizations.

2.3. X-ray crystallography

X-ray intensity data from a colorless needle of compound **1** and of compound **2** were measured at 150(2) K and at 100(2) K, respectively using a Bruker SMART APEX diffractometer (Mo K_α radiation, $\lambda = 0.71073$ Å)[40]. Raw area detector data frame processing was performed with the SAINT+ and SADABS programs[40]. Final unit cell parameters were determined by least-squares refinement of 3884 (compound **1**) and 9214 (compound **2**) reflections from the data set. Direct methods structure solution, difference Fourier calculations and full-matrix least-squares refinement against F^2 were performed with SHELXTL[41].

Compound **1** crystallizes in the monoclinic system. The space groups $P2_1$ and $P2_1/m$ were indicated by the pattern of systematic absences in the intensity data. $P2_1$ was eventually confirmed by achieving a successful and stable solution and refinement of the data. The space group choice was further checked with the ADDSYM program implemented in PLATON, which found no missed symmetry elements[42]. The asymmetric unit consists of two unique bismuth atoms, two oxide ions and one pydc ligand. All non-hydrogen atoms were refined with anisotropic displacement parameters. Hydrogen atoms were placed in geometrically idealized positions and included as riding atoms. The final absolute structure (Flack) parameter is $-0.02(2)$. The largest residual electron density peak is $+1.88\ e^-/Å^3$, located 0.78 Å from Bi1.

Compound **2** crystallizes in the space group $P2_1$ as determined by the pattern of systematic absences in the intensity data and the known chirality of the 1*R*3*S*-camphorate ligand used. The absolute structure (Flack) parameter after the final refinement cycle was 0.007(8). The asymmetric unit consists of four bismuth atoms, four sodium atoms, eight 1*R*3*S*-camphorate ligands and several disordered electron density peaks surrounding the sodium atoms, which were modeled either as ethanol molecules or as oxygen atoms of water molecules. The refinement was complicated by extensive disorder of four of the eight camphorate ligands, one sodium atom (Na4) and the solvent species (ethanol and water) which are either coordinated to sodium atoms or located in interstitial regions. The disordered camphorate ligands are: C41–C50, C51–C60, C61–C70, and C71–C80. Only the central part of these ligands is disordered; the carboxylate groups are not disordered. The disorder takes the form of a two-fold rotation perpendicular to a vector passing through atoms C(n1) and C(n3) of each ligand (n=4–7), and as such the stereochemistry of each disorder component is the same (i.e., 1*R*3*S*). The sum of the occupancies of the two orientations (suffix *A* or *B*) was constrained to sum to unity. Atoms C(n1) and C(n3) (n=4–7) are common to each disorder component. The disorder fractions refined to: C41–C50 *A*/*B*=0.44(2)/0.56(2); C51–C60 *A*/*B*=0.63(1)/0.37(1); C61–C70 *A*/*B*=0.43(1)/0.57(1); C71–C80 *A*/*B*=0.66(1)/0.34(1). These species were refined isotropically. For C41–C50 *A*, C51–C60 *A*/*B* and C71–C80 *A*/*B*, disordered atoms of each ligand was assigned a common displacement parameter. The geometry of each disorder component was restrained to be similar to that of the well-behaved ligand C31–C40. The solvent species in particular proved resistant to sensible disorder modeling. Near Na1, one ethanol molecule disordered over two sites was refined (oxygen atoms O81*A*, occupancy 0.59(2) and O81*B*, 0.41(2)). Around Na2, the disorder model consists of one ethanol (O86*A*, 0.67(1)), a coordinated water molecule (O86*B*, 0.33(1)) and a non-coordinated water (O87, 0.33(1)). Near Na3, one ethanol (O82*A*, 0.65(1)), three coordinated waters (O82*B*, 0.35(1); O84, 0.54(2); O85, 0.46(2)) and one non-coordinated water (O83, 0.35(1)) were refined. Sodium atom Na4 is itself disordered over a split position with refined population Na4*A*/Na4*B*=0.78(1)/0.22(1). The electron density near the Na4 sites was modeled as one ethanol bonded to Na4*A* (O88*A*, 0.78(1)), one water bonded to Na4*B* (O89*B*, 0.22(1)), and a non-coordinated water (O90, 0.78(1)). Populations of these molecules were linked to the sodium atom to which they are attached. During the modeling of the solvent disorder, care was taken to ensure the sum of the occupancies of partially occupied atoms in close proximity to one another was equal to or less than unity. The persistence of several scattered electron density peaks in the vicinity of these species indicates more complex disorder than described by the reported model. For this reason the water/ethanol content and distribution should be regarded as approximate. Non-disordered, non-hydrogen atoms were refined with anisotropic displacement parameters. Hydrogen atoms of the camphorate ligands were placed in geometrically idealized positions and included as riding atoms. No hydrogen atoms of the water and ethanol molecules were located or calculated.

2.4. Powder X-ray diffraction

A ground mixture of polycrystalline powders and needle crystals of compound **2** was used to collect powder X-ray diffraction patterns using a Rigaku Ultima IV Powder Diffractometer equipped with high speed DTex detector and Cu K_α radiation (λ=1.5418 Å) over the 2θ range of 5°–30°, with a step size of 0.02° and a scan speed of 2°/min. The measured pattern of the compound was compared with the diffraction patterns generated by CrystalMaker® 8.0. using the single crystal data of compound **2**.

2.5. SHG measurement

A modified Kurtz-NLO system [43], using a pulsed Nd:YAG laser with a wavelength of 1064 nm, was used to perform the powder SHG measurements at room temperature. The methodology and instrumentation details have been published elsewhere [44]. Attributable to particle size dependence, the crystalline samples were ground and sieved into distinct particle size ranges (10–20, 20–45, 45–63, 63–75, 75–90, 90–120, and 120–150 μm). In order to evaluate relative SHG efficiencies of the measured samples with known SHG materials, crystalline α-SiO_2 was also ground and sieved into the same particle size ranges. No index matching fluid was used in this experiment.

3. Results and discussion

3.1. Structure description

The reactions of pyridine-2, 5-dicarboxylic acid (H_2pydc) with $Bi(NO_3)_3\cdot 5H_2O$ under hydrothermal conditions resulted in compounds Bi_2O_2(pydc), compound **1**, which crystallizes in a 3D structure that contains Bi_2O_2 chains that are connected into a 3D structure via the pydc ligands. Relevant crystallographic data from the single-crystal structure refinement are found in Table 1. Selected interatomic distances are summarized in Table 2.

Compound **2**, Bi_4Na_4(1*R*3*S*-cam)$_8$(EtOH)$_{3.1}$(H_2O)$_{3.4}$, was obtained from the reactions of 1*R*3*S*-camphoric acid with $Bi(NO_3)_3\cdot 5H_2O$ and NaOH under solvothermal conditions. Its structure, a true 3D coordination polymer, was determined via single crystal X-ray diffraction. Relevant crystallographic data from the single-crystal structure refinement are found in Table 1. Selected interatomic distances are summarized in Table 3.

Fig. 1(a) depicts the asymmetric unit cell and atom labels of Bi_2O_2(pydc), which consists of two unique bismuth atoms, two oxo-oxygen atoms (presumably from the thermal degradation of

Table 2
Representative bond lengths (Å) and bond angles (°) of compound **1**.

Bi(1)–O(5)	2.106(8)
Bi(1)–O(2)#1	2.420(8)
Bi(1)–O(3)#2	2.489(8)
Bi(1)–O(1)	2.498(10)
Bi(1)–O(5)#3	2.502(9)
Bi(1)–O(6)	2.523(8)
Bi(1)–N(1)	2.827(11)
Bi(1)–Bi(2)	3.5424(6)
Bi(2)–O(5)	2.061(8)
Bi(2)–O(6)#4	2.176(8)
Bi(2)–O(6)#5	2.303(9)
Bi(2)–O(6)	2.318(9)
Bi(2)–O(4)#2	2.737(11)
Bi(2)–O(2)#6	2.787(9)
Bi(2)–Bi(2)#7	3.5794(7)
O(5)–Bi(1)–O(2)#1	84.2(3)
O(5)–Bi(1)–O(3)#2	88.1(3)
O(5)–Bi(1)–O(1)	89.9(3)
O(2)#1–Bi(1)–O(1)	71.8(3)
O(5)–Bi(1)–N(1)	81.3(3)
O(3)#2–Bi(1)–N(1)	70.8(3)
O(1)–Bi(1)–N(1)	59.8(3)

Symmetry transformations used to generate equivalent atoms.
#1 −x+1,y−1/2,−z #2 −x+1,y−1/2,−z+1 #3 x,y−1,z.
#4 −x,y+1/2,−z #5 x,y+1,z #6 x−1,y,z #7 −x,y−1/2,−z.
#8 −x+1,y+1/2,−z #9 −x+1,y+1/2,−z+1.

Table 1
Crystal data and structure refinement of compound **1** and **2**.

Compound	**1**	**2**
Empirical formula	C_7 H_3 Bi_2 N O_6	$C_{86.20}H_{112}$ Bi_4 Na_4 $O_{38.45}$
Formula weight	615.06	2691.24
Temperature	150(2) K	100(2) K
Wavelength	0.71073 Å	0.71073 Å
Crystal system	Monoclinic	Monoclinic
Space group	$P2_1$	$P2_1$
Unit cell dimensions	a=9.6479(9) Å, α=90°	a=19.0855(7) Å, α=90°
	b=4.2349(4) Å, β=109.587(1)°	b=13.7706(5) Å, β=90.701(1)°
	c=11.9615(11) Å, γ=90°	c=19.2429(7) Å, γ=90°
Volume	460.44(7) Å^3	5057.0(3) Å^3
Z	2	2
Density (calculated)	4.436 Mg/m^3	1.767 Mg/m^3
Absorption coefficient	38.179 mm^{-1}	7.039 mm^{-1}
F(000)	532	2626
Crystal size	0.26 × 0.08 × 0.05 mm^3	0.28 × 0.08 × 0.06 mm^3
Theta range for data collection	1.81 to 27.92°	1.06 to 26.42°
Index ranges	−12 <=h<=12, −5 <=k<=5,−15 <=l<=15	−23 <=h<=23, −17 <=k<=17,−24 <=l<=24
Reflections collected	6,407	70,778
Independent reflections	2205 [R(int)=0.0330]	20732 [R(int)=0.0828]
Completeness to theta	100.0%	99.9%
Max. and min. transmission	1.0000 and 0.1813	1.0000 and 0.5476
Data/restraints/parameter	2205/ 1/ 145	20732/ 997/ 1040
Absolute structure (Flack) parameter	0.02(2)	0.007(8)
Goodness-of-fit on F^2	1.156	1.042
Final R indices [I > 2sigma(I)]	R1=0.0286, wR2=0.0756	R1=0.0546, wR2=0.1130
R indices (all data)	R1=0.0294, wR2=0.0760	R1=0.0739, wR2=0.1216

Table 3
Representative bond lengths (Å) and bond angles (°) of compound **2**.

Bi(1)–O(23)	2.207(8)
Bi(1)–O(3)	2.213(8)
Bi(1)–O(2)#1	2.325(10)
Bi(1)–O(12)	2.359(10)
Bi(1)–O(1)#1	2.713(9)
Bi(1)–O(4)	2.743(9)
Bi(2)–O(53)	2.203(8)
Bi(2)–O(42)#2	2.219(9)
Bi(2)–O(44)	2.361(9)
Bi(2)–O(31)	2.362(9)
Bi(2)–O(41)#2	2.672(8)
Bi(2)–O(32)	2.694(9)
Bi(2)–O(54)	2.706(8)
Bi(3)–O(34)	2.225(8)
Bi(3)–O(63)#3	2.279(8)
Bi(3)–O(52)#4	2.352(9)
Bi(3)–O(61)	2.367(8)
Bi(3)–O(33)	2.592(8)
Bi(3)–O(64)#3	2.629(8)
Bi(3)–O(51)#4	2.742(10)
Bi(4)–O(14)	2.248(8)
Bi(4)–O(71)	2.257(7)
Bi(4)–O(21)#4	2.287(8)
Bi(4)–O(73)#5	2.364(9)
Bi(4)–O(13)	2.614(9)
Bi(4)–O(72)	2.708(9)
Na(1)–O(81A)	2.26(2)
Na(1)–O(11)	2.282(10)
Na(1)–O(81B)	2.29(4)
Na(1)–O(41)#2	2.313(10)
Na(1)–O(43)	2.318(10)
Na(1)–O(24)	2.328(11)
Na(2)–O(86A)	2.20(2)
Na(2)–O(64)#3	2.283(9)
Na(2)–O(13)#7	2.327(10)
Na(2)–O(62)	2.335(10)
Na(2)–O(22)#8	2.341(10)
Na(2)–O(86B)	2.69(5)
Na(2)–Bi(4)#7	3.702(5)
Na(3)–O(84)	2.11(3)
Na(3)–O(33)	2.216(10)
Na(3)–O(74)#1	2.275(13)
Na(3)–O(82B)	2.31(5)
Na(3)–O(82A)	2.31(2)
Na(3)–O(72)#7	2.369(11)
Na(3)–O(85)	2.79v4)
Na(3)–Bi(4)#7	3.820(7)
Na(4A)–Na(4B)	1.39(4)
Na(4A)–O(54)	2.233(11)
Na(4A)–O(4)	2.311(13)
Na(4A)–O(1)#1	2.314(13)
Na(4A)–O(88A)	2.395(9)
Na(4B)–O(32)	2.16(4)
O(23)–Bi(1)–O(3)	77.6(3)
O(23)–Bi(1)–O(2)#1	78.3(4)
O(3)–Bi(1)–O(2)#1	82.0(3)
O(23)–Bi(1)–O(12)	84.0(4)
O(3)–Bi(1)–O(12)	75.8(3)
O(53)–Bi(2)–O(42)#2	78.8(3)
O(53)–Bi(2)–O(44)	78.0(3)
O(42)#2–Bi(2)–O(44)	81.3(4)
O(53)–Bi(2)–O(31)	85.1(3)
O(42)#2–Bi(2)–O(31)	77.0(3)
O(34)–Bi(3)–O(63)#3	81.6(3)
O(34)–Bi(3)–O(52)#4	82.7(3)
O(63)#3–Bi(3)–O(52)#4	74.8(3)
O(34)–Bi(3)–O(61)	78.3(3)
O(63)#3–Bi(3)–O(61)	80.1(3)
O(14)–Bi(4)–O(71)	77.5(3)
O(14)–Bi(4)–O(21)#4	81.3(3)
O(71)–Bi(4)–O(21)#4	77.1(3)
O(14)–Bi(4)–O(73)#5	75.5(3)
O(71)–Bi(4)–O(73)#5	81.9(4)
O(81A)–Na(1)–O(11)	127.0(8)
O(81A)–Na(1)–O(81B)	19.1(10)
O(11)–Na(1)–O(81B)	146.1(10)
O(81A)–Na(1)–O(41)#2	104.4(7)

Table 3 (*continued*)

O(11)–Na(1)–O(41)#2	84.0(4)
O(86A)–Na(2)–O(64)#3	98.1(6)
O(86A)–Na(2)–O(13)#7	101.4(6)
O(64)#3–Na(2)–O(13)#7	160.5(4)
O(86A)–Na(2)–O(62)	145.6(7)
O(64)#3–Na(2)–O(62)	83.9(3)
O(13)#7–Na(2)–O(62)	79.2(4)
O(84)–Na(3)–O(33)	71.0(8)
O(84)–Na(3)–O(74)#1	137.6(10)
O(33)–Na(3)–O(74)#1	98.3(5)
O(84)–Na(3)–O(82B)	65.6(14)
O(33)–Na(3)–O(82B)	102.3(11)
O(74)#1–Na(3)–O(82B)	153.9(13)
Na(4B)–Na(4A)–O(54)	83.4(12)
Na(4B)–Na(4A)–O(4)	71.0(13)
O(54)–Na(4A)–O(4)	122.5(5)
Na(4B)–Na(4A)–O(1)#1	141.6(14)
O(54)–Na(4A)–O(1)#1	93.2(5)
O(4)–Na(4A)–O(1)#1	79.1(4)
Na(4B)–Na(4A)–O(88A)	91.1(13)

Symmetry transformations used to generate equivalent atoms.
#1 $-x+1,y-1/2,-z+1$ #2 $-x,y+1/2,-z+1$ #3 $-x,y+1/2,-z$.
#4 $x,y+1,z$ #5 $-x+1,y-1/2,-z+2$ #6 $x,y,z+1$.
#7 $x,y,z-1$ #8 $x,y+1,z-1$ #9 $-x+1,y+1/2,-z+1$.
#10 $x,y-1,z$ #11 $x,y-1,z+1$ #12 $-x,y-1/2,-z+1$.
#13 $-x,y-1/2,-z$ #14 $-x+1,y+1/2,-z+2$.

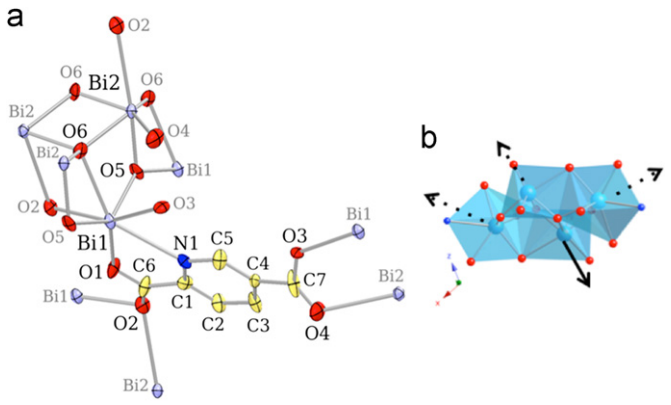

Fig. 1. (a) Asymmetric structure of compound **1**, Bi_2O_2(pydc) (pydc=pyridine-2, 5-dicarboxylate). Displacement ellipsoids are drawn at the 50% probability level. Hydrogen atoms are omitted. Symmetry-equivalent atoms are labeled in gray. (b) The bismuth centered polyhedra of the compound **1** with arrows indicating the approximate directions of the dipole moments (dotted lines indicate that the arrows are behind the polyhedra). Bi=blue polyhedra, O=red spheres, N=dark blue spheres. (For interpretation of the references to color in this figure legend, the reader is referred to the web version of this article.)

hydroxo-salt) [45] ions and one pydc ligand. The overall structure is built around Bi_2O_2 chains extended along the *y*-axis. The nitrogen and oxygen atoms of the pydc ligands as well as two oxo-oxygen atoms complete the coordination sphere around the bismuth cations in the Bi_2O_2 chains to form $Bi(1)O_5N$, $Bi(2)O_6$, $Bi(2)O_6$ and $Bi(1)O_5N$ polyhedra, Fig. 1(b), with Bi–O distances ranging from 2.061(8) to 2.787(9) Å, and a Bi–N distance of 2.827(11) Å. All the Bi^{3+} distorted polyhedra are hemidirected and contain stereochemically-active lone pairs shown in Fig. 1(b). This Bi_2O_2 chain consists of a chain of corner-shared $Bi(1)O_5N$ distorted pentagonal bipyramids (A chain), which share a common edge with another chain of $Bi(2)O_6$ distorted octahedra (B chain) forming an AB chain, that in turn shares edges with another AB chain with a different spatial orientation (A′B′ chain) forming an overall ABA′B′ chain (Fig. S1, Supporting Information). The AB and A′B′ chains are related by a two-fold symmetry along the *x*-axis. These ABA′B′ chains are bridged by the pydc ligands to

form a 2D structure (Fig. S2, Supporting Information) in the *x*-direction as well as a chiral 3D structure in the *z*-direction as shown in Fig. 2. The chirality arises from the pydc ligands within one unit cell where the structure is related by 2_1 symmetry along the *z*-axis without an inversion center (Fig. 2). The bridging carboxylates, both in the *x* and *z* directions, exists in conjunction with weak π–π stacking of pyridine rings (distance between the rings is 4.235 Å).

The asymmetric unit and atom labeling of compound **2** is shown in Fig. 3(a), which consists of four bismuth atoms, four sodium atoms, eight 1*R*3*S*-camphorate ligands (1*R*3*S*-cam) and several disordered electron density peaks surrounding the sodium atoms, which were modeled either as ethanol molecules or as oxygen atoms of water molecules. Note that four of the eight independent 1*R*3*S*-cam ligands are rotationally disordered over two orientations. Fig. S3 (Supporting Information) shows the disordered structure, which involves a two-fold rotation roughly perpendicular to the plane in view (b), affecting the four 1*R*3*S*-cam ligands, C41–C50, C51–C60, C61–C70, and C71–C80. The carboxylate groups are not disordered as C(*n*1) and C(*n*3) are common to each disorder component.

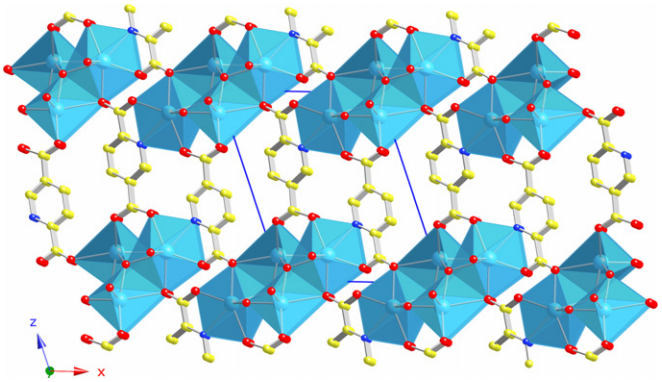

Fig. 2. 3D structure of compound **1** emphasizing the 2_1 symmetry along the *z*-direction. Bi=blue polyhedra, O=red spheres, N=dark blue spheres, C=yellow spheres. (For interpretation of the references to color in this figure legend, the reader is referred to the web version of this article.)

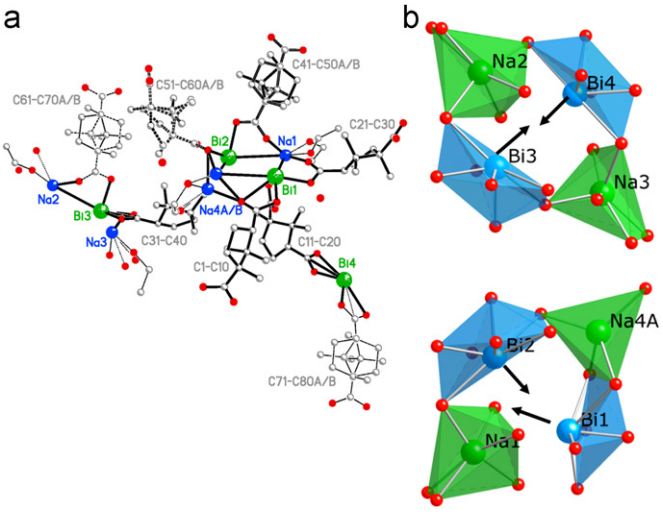

Fig. 3. (a) Asymmetric unit of compound **2**, $Bi_4Na_4(1R3S\text{-cam})_8(EtOH)_{3.1}(H_2O)_{3.4}$ (1*R*3*S* cam=1*R*3*S*-camphoric acid). (b) The bismuth centered polyhedra of **2** with arrows indicating the approximate directions of the dipole moments (dotted lines indicate that the arrows are behind the polyhedra). Bi=blue polyhedra, O=red spheres, N=dark blue spheres. (For interpretation of the references to color in this figure legend, the reader is referred to the web version of this article.)

The coordination sphere around the four bismuth cations, $Bi(1)O_6$, $Bi(2)O_7$, $Bi(2)O_7$, and $Bi(4)O_6$, are made up of O from 1*R*3*S*-cam ligands to form hemidirected polyhedra of nido pentagonal bipyramid, capped nido pentagonal bipyramid, capped nido pentagonal bipyramid, and capped nido octahedron, respectively (Fig. 3(b)). Such distorted polyhedra have typical stereochemically active lone pair characteristics: relatively short Bi–O distances ranging from 2.207(8) to 2.367(8) Å, and relatively long Bi–O distances ranging from 2.592(8) to 2.743(9) Å, as well as bond angles that are less than 90° (ranging from 50.8(3) to 85.5(3)°), listed in Table 3. The presence of stereochemically-active lone pairs is commonly observed in bismuth-based coordination compounds [25, 45–46].

In the case of the sodium coordination environment, oxygens from both the 1*R*3*S*-cam ligands and ethanol/water complete the coordination sphere around the four sodium cations (without regard to the presence of disordered atoms), $Na(1)O_6$, $Na(2)O_6$, $Na(3)O_6$, and $Na(4)O_4$, forming irregular octahedra, irregular monocapped square pyramids, and irregular tetrahedra (Fig. 3(b)).

The structure contains zigzag chains that extend along the *z*-direction when viewed down the *y*-axis, as shown in Fig. S4 (Supporting Information). However, when rotated 90° about the (−) *y*-axis, it becomes apparent that this is actually a 2D structure due to the bridging 1*R*3*S*-cam ligands connecting the chains along the *y*-direction (Fig. S5, Supporting Information). These 2D structures are stacked on top of each in the *x*-direction. The Na cations complete the 3D structure by connecting the stacked 2D layers along the *x*-direction as shown in Fig. S6 (Supporting Information).

Fig. S6 (Supporting Information) depicts the structure of **2** built from the above-mentioned polyhedra sharing corners to form four-membered rings, Bi(3)–Na(2)–Bi(4)–Na(3) polyhedra, and Bi(1)–Na(1)), for Bi(1)–Na(1)–Bi(2)–Na(4) polyhedra. These two rings are adjacent to each other (along with connecting ligands) and create an overall infinite 2_1 chiral, helical chain extending along the *y*-direction (Fig. 4). For clarity, Fig. S7 (Supporting Information) depicts the 2_1 relationship.

3.2. Powder X-ray diffraction

Powder X-ray diffraction can provide phase purity information and, for example, reveal the presence or absence of polymorphs. The purity of compound **2**, mixture of polycrystalline powder and needle crystals, was checked using powder X-ray diffraction. The powder diffraction patterns that were collected on ground mixtures of polycrystalline powder and needle crystals of compound **2** match the calculated patterns based on the single crystal structure as shown in Fig. S8 (Supporting Information). This demonstrates that the reaction products are single phase, that within the resolution of powder X-ray diffraction, no additional polymorph is present, and that, within detection limits, no unreacted starting material remains in the samples.

3.3. Second harmonic generation

Second harmonic generation (SHG) materials, or commonly known as frequency doubling materials, are important nonlinear optic (NLO) materials that are capable of converting a specific wavelengths of light into half of its original value. There is increasing interest in NLO materials based on enantiomerically pure metal-organic coordination polymer possessing polar space groups, some of which are reported to exhibit both SHG and ferroelectric properties [34–43]. Based on this comprehensive list and our search of the literature, it appears that **1** and **2** are the first examples of polar, non-centrosymmetric 3D bismuth-based coordination polymers synthesized by employing unsymmetric ligands (compound **1**) or chiral ligands (compound **2**), together

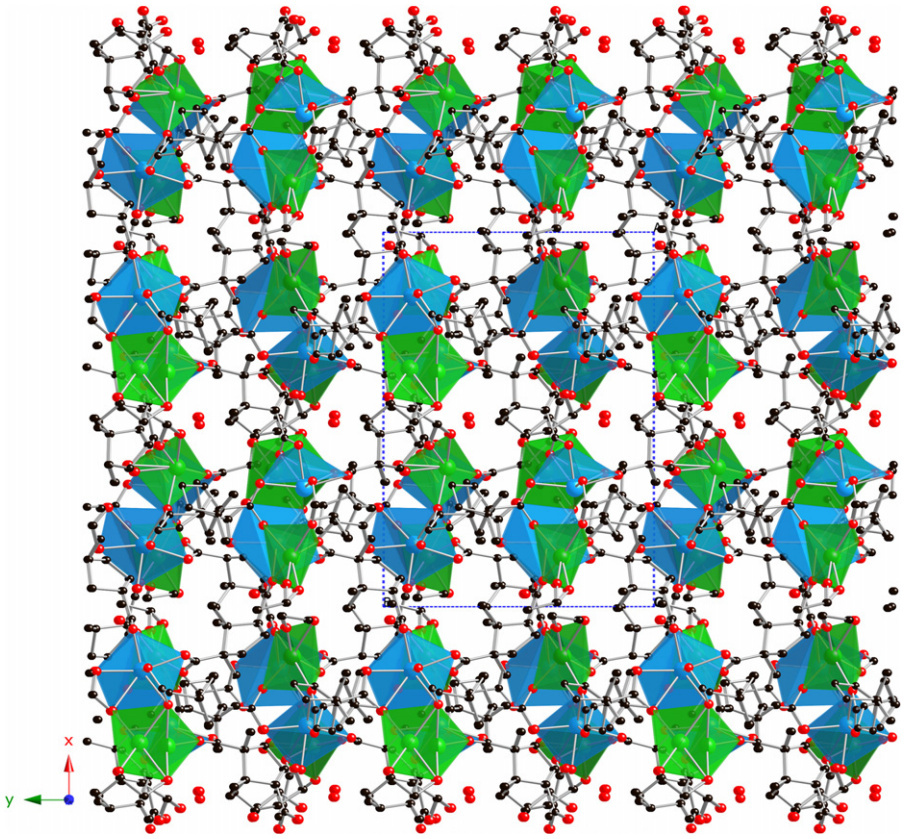

Fig. 4. Overall 3D structure of **2** emphasizing the 2_1 symmetry along the *y*-direction. Bi=blue polyhedra, Na=green polyhedra, O=red spheres, C=black spheres. (For interpretation of the references to color in this figure legend, the reader is referred to the web version of this article.)

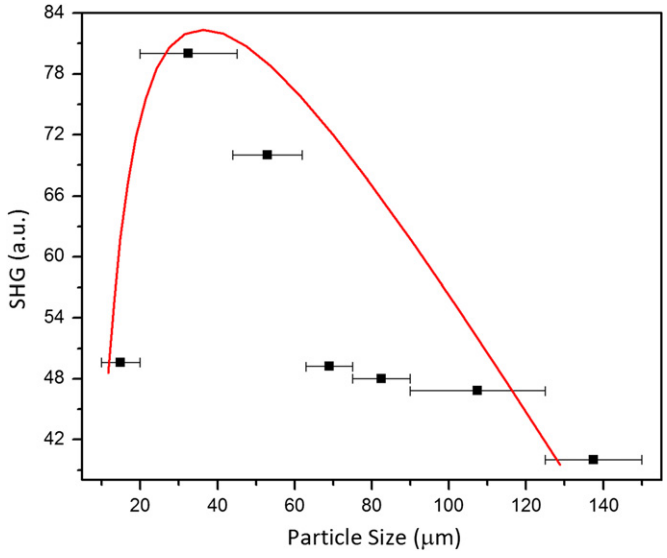

Fig. 5. SHG intensity curve as function of particle size of compound **1**. The red line is to guide the eye, and does not represent a curve fit. (For interpretation of the references to color in this figure legend, the reader is referred to the web version of this article.)

with metals that often exhibit stereochemically-active lone pairs, such as Bi^{3+}.

Both of the reported compounds crystallize in the polar and non-centrosymmetric space group $P2_1$ (# 4), which satisfies the structural requirement for exhibiting SHG effect. Powder SHG measurements on compounds **1** and **2** indicate that they are SHG active and SHG inactive, respectively. The existence of a non-centrosymmetric space group allows SHG activity, but does not require the existence of SHG activity. Compound **2** is an example of a material that is non-centrosymmetric, but hat does not exhibit SHG activity. Interestingly, however, we observe white light emission during the SHG measurement for compound **2**. Compound **1** is SHG active with an efficiency of ~80 × α-SiO_2 for particles ranging in size from 45 to 63 μm. Additional SHG measurements, particle size vs. SHG efficiency, indicated that compound 1 is type 1 non-phase-matchable (see Fig. 5). This indicates that compound **1** falls into the class C of SHG materials as defined by Kurtz and Perry. [43] The moderate SHG efficiency of compound **1** can be attributed to the partial alignment of dipole moments of the distorted Bi polyhedra as shown in Fig. 1(b), which in turn results in partial "constructive addition" and a moderate (80 × α-SiO_2) SHG efficiency.

4. Conclusion

We have successfully synthesized two homochiral 3D metal-organic coordination polymers by combining unsymmetric ligands (H_2pydc) or homochiral ligands (1R3S-cam) and main group metals with stereochemically-active lone pairs (Bi^{3+}). The resulting compound **1**, Bi_2O_2(pydc), consists of Bi_2O_2 chains that are connected into 2D layers and pillared into a true 3D coordination polymer via pydc linking ligands. The compound is non-phase-matching with a moderate SHG efficiency. Compound **2**, Bi_4Na_4(1*R*3*S*-cam)$_8$(EtOH)$_{3.1}$(H_2O)$_{3.4}$, is an enantiomerically pure 3D coordination polymers that consists of bismuth-based sheets that are connected into a 3D structure by the sodium cations located in between the layers. Although compound **2**

crystallizes in a polar and non-centrosymmetric space group, it is, however, SHG inactive.

Crystallographic data for the structures reported in this paper have been deposited with the Cambridge Crystallographic Data Center as supplementary publication no. CCDC 859456 compound **1** and 859457 compound **2**. These data can be obtained free of charge via www.ccdc.cam.ac.uk/data_request/cif, or by emailing data_request@ccdc.cam.ac.uk, or by contacting The Cambridge Crystallographic Data Center, 12, Union Road, Cambridge CB2 1EZ, UK; fax: +44 1223 336033.

Acknowledgments

Financial support for this research was provided in part by the United States Air Force award No. FA9550-08-10377 and in part by National Science Foundation through Grant CHE-0714439. JY and PSH thank the Welch Foundation (Grant E-1457) and the Texas Center for Superconductivity for support.

Appendix A. Supplementary material

Supplementary data associated with this article can be found in the online version at doi:10.1016/j.jssc.2012.01.038.

References

[1] J.J. Perry IV, J.A. Perman, M.J. Zaworotko, Chem. Soc. Rev. 38 (2009) 1400–1417.
[2] O.M. Yaghi, D.A. Richardson, G. Li, E. Davis, T.L. Groy, Mater. Res. Soc. Symp. Proc. 371 (1995) 15–19.
[3] O.M. Yaghi, H. Li, J. Am. Chem. Soc. 117 (1995) 10401–10402.
[4] S.-i. Noro, S. Kitagawa, M. Kondo, K. Seki, Angew. Chem. Int. Ed. 39 (2000) 2082–2084.
[5] S. Shimomura, S. Horike, S. Kitagawa, Stud. Surf. Sci. Catal. 170B (2007) 1983–1990.
[6] O.M. Yaghi, M. O'Keeffe, N.W. Ockwig, H.K. Chae, M. Eddaoudi, J. Kim, Nature 423 (2003) 705–714.
[7] M. Eddaoudi, D.B. Moler, H. Li, B. Chen, T.M. Reineke, M. O'Keeffe, O.M. Yaghi, Acc. Chem. Res. 34 (2001) 319–330.
[8] A.F. Wells, Acta Crystallogr. 7 (1954) 535–544.
[9] A.F. Wells, Acta Crystallogr. 7 (1954) 545–554.
[10] A.F. Wells, Three Dimensional Nets and Polyhedra, Wiley, New York, 1977.
[11] A.F. Wells, Structural Inorganic Chemistry, Oxford University Press, London, 1984.
[12] A.C. Wibowo, M.D. Smith and H.-C. zur Loye, Chem. Commun. (2011) 10.1039/c1cc11720c.
[13] H. Furukawa, N. Ko, Y.B. Go, N. Aratani, S.B. Choi, E. Choi, A.O. Yazaydin, R.Q. Snurr, M. O'Keeffe, J. Kim, O.M. Yaghi, Science 329 (2010) 424–428.
[14] M. T. K., S. Kitagawa, Pure Appl. Chem. 79 (2007) 2155–2177.
[15] D.J. Collins, H.-C. Zhou, J. Mater. Chem. 17 (2007) 3154–3160.
[16] M. Eddaoudi, H. Li, O.M. Yaghi, J. Am. Chem. Soc. 122 (2000) 1391–1397.
[17] J.S. Seo, D. Whang, H. Lee, S.I. Jun, J. Oh, Y.J. Jeon, K. Kim, Nature 404 (2000) 982–986.
[18] P.M. Foster, A.K. Cheetham, Top. Catal. 24 (2003) 79–86.
[19] C.-D. Wu, A. Hu, L. Zhang, W. Lin, J. Am. Chem. Soc. 127 (2005) 8940–8941.
[20] S.-H. Cho, B. Ma, S.T. Nguyen, J.T. Hupp, T.E. Albrecht-Schmitt, Chem. Commun. 24 (2006) 2563–2565.
[21] P. Dechambenoit and J.R. Long, Chem. Soc. Rev. 10.1039/c0cs00167h.
[22] S. Kitagawa, K. Uemura, Chem. Soc. Rev. 34 (2005) 109–119.
[23] B. Chen, L. Wang, F. Zapata, G. Qian, E.B. Lobkovsky, J. Am. Chem. Soc. 130 (2008) 6718–6719.
[24] M. Xue, G. Zhu, Y. Li, X. Zhao, Z. Jin, E. Kang, S. Qiu, Cryst. Growth Des. 8 (2008) 2478–2483.
[25] A.C. Wibowo, S.A. Vaughn, M.D. Smith, H.-C. zur Loye, Inorg. Chem. 49 (2010) 11001–11008.
[26] Y. Liu, G. Li, X. Li, Y. Cui, Angew. Chem. Int. Ed. 46 (2007) 6301–6304.
[27] H.-B. Cui, Z. Wang, K. Takahashi, Y. Okano, H. Kobayashi, A. Kobayashi, J. Am. Chem. Soc. 128 (2006) 15074–15075.
[28] P. Jain, V. Ramachandran, R.J. Clark, H.D. Zhou, B.H. Toby, N.S. Dalal, H.W. Kroto, A.K. Cheetham, J. Am. Chem. Soc. 131 (2009) 13625–13627.
[29] W. Zhang, H.-Y. Ye, H.-L. Cai, J.-Z. Ge, R.-G. Xiong, S.D. Huang, J. Am. Chem. Soc. 132 (2010) 7300–7302.
[30] G.-C. Xu, X.-M. Ma, L. Zhang, Z.-M. Wang, S. Gao, J. Am. Chem. Soc. 132 (2010) 9588–9590.
[31] H.-B. Cui, K. Takahashi, Y. Okano, H. Kobayashi, Z. Wang, A. Kobayashi, Angew. Chem. Int. Ed. 44 (2005) 6508–6512.
[32] H.-B. Cui, B. Zhou, L.-S. Long, Y. Okano, H. Kobayashi, A. Kobayashi, Angew. Chem. Int. Ed. 47 (2008) 3376–3380.
[33] W. Zhang, Y. Cai, R.-G. Xiong, H. Yoshikawa, K. Awaga, Angew. Chem. Int. Ed. 49 (2010) 6608–6610.
[34] W. Xu, W. Liu, F.-Y. Yao, Y.-Q. Zheng, Inorg. Chim. Acta 365 (2011) 297–301.
[35] J.-D. Lin, X.-F. long, P. Lin, S.-W. Du, Cryst. Growth Des. 10 (2010) 146–157.
[36] Y.-T. Wang, G.-M. Tang, Y.-Q. Wei, T.-X. Qin, T.-D. Li, C. He, J.-B. Ling, X.-F. Long, S.W. Ng, Cryst. Growth Des. 10 (2010) 25.
[37] Y.-Q. Wei, K. Wu, J. He, W. Zheng, X. Xiao, Cryst. Eng. Commun. 13 (2011) 52–54.
[38] Q.-Y. Liu, Y.-L. Wang, Z.-M. Shan, R. Cao, Y.-L. Jiang, Z.-J. Wang, E.-L. Yang, Inorg. Chem. 49 (2010) 8191–8193.
[39] T. Hang, W. Zhang, H.-Y. Ye, R.-G. Xiong, Chem. Soc. Rev. (2011). doi:10.1039/c0cs00226g.
[40] SMART Ver. 5.630, SAINT+ Ver. 6.45 and SADABS Ver. 2.10; Bruker Analytical X-ray Systems, Inc, Wisconsin, Madison, 2003.
[41] G.M. Sheldrick, SHELXTL Ver. 6.14 edn., Bruker Analytical X-ray Systems, Inc, Madison, Wisconsin, 2003.
[42] (a) A.L. Spek, Acta Crystallogr., Sect. A 46 (1990) C34;
(b) A. Platon, Multipurpose Crystallographic Tool, Utrecht University, Utrecht, The Netherlands, Spek, A. L., 1998.
[43] S.K. Kurtz, T.T. Perry, J. Appl. Phys. 39 (1968) 3798.
[44] K.M. Ok, E.O. Chi, P.S. Halasyamani, Chem. Soc. Rev. 35 (2006) 710–717.
[45] A.C. Wibowo, M.D. Smith, H.-C. zur Loye, Cryst. Eng. Commun. 13 (2011) 426–429.
[46] V. Stavila, K.H. Whitmire, I. Rusakova, Chem. Mater. 21 (2009) 5456.